Astronomy & Astrophysics manuscript no. output
June 30, 2026

Ensemble pulsational characteristics of eclipsing binaries containing β Cep stars observed by the TESS mission

C. I. Eze [1,2,3,⋆], G. Handler [1], M. Vanrespaille [3] A. Kemp [3], A. Tkachenko [3], D. M. Bowman [4,3], and C. Aerts [3,5,6]

[1] Nicolaus Copernicus Astronomical Centre, Polish Academy of Sciences, Bartycka 18, PL-00-716 Warsaw, Poland
e-mail: cheze@camk.edu.pl
[2] Department of Physics and Astronomy, Faculty of Physical Sciences, University of Nigeria, Nsukka, Nigeria
[3] Institute of Astronomy, KU Leuven, Celestijnenlaan 200D, 3001 Leuven, Belgium
[4] School of Mathematics, Statistics and Physics, Newcastle University, Newcastle upon Tyne, NE1 7RU, UK
[5] Department of Astrophysics, IMAPP, Radboud University Nijmegen, PO Box 9010, 6500 GL Nijmegen, The Netherlands
[6] Max Planck Institut für Astronomie, Königstuhl 17, 69117 Heidelberg, Germany

June 30, 2026

ABSTRACT

Context. Massive pulsators in eclipsing binaries are ideal candidates for studying interior mixing and angular momentum transport in massive stars. Eclipsing binaries particularly provide precise and model-independent stellar parameters, which are subsequently used with asteroseismic constraints to derive stellar interior properties, such as interior rotation, mass of the convective core, and interior mixing parameters.
Aims. This study investigates the pulsational characteristics and their impact on the structure and evolution of β Cep pulsators in eclipsing binaries.
Methods. We analyse an ensemble of 65 β Cep stars in eclipsing binaries, identify rotationally split modes where possible, and statistically derive the dependence of pulsational properties on binary orbital parameters using a Bayesian inference framework. The interior properties of the systems were also derived using pre-computed grids of stellar structure models with MESA and associated pulsation frequencies using SтORM and an asteroseismic routine that tracks the age and rotation of the star in the entire β Cep instability region.
Results. Interior rotation rates are derived for 14 systems that exhibit rotational mode splitting. We find differential rotation in HD 112485 and quasi-solid body rotation for the other system primaries. Detailed forward asteroseismic modelling was conducted for HD 112485 and EK Cru to deduce their seismic and core properties, as well as their evolutionary state. HD 112485 is one of the least evolved β Cep stars asteroseismically modelled to date, with a core hydrogen mass fraction $X_c = 0.479^{+0.009}_{-0.010}$. The two reproduced zonal modes in HD 112485 are the first radial-order dipole pressure mode and the second radial-order quadrupole gravity mode, while the zonal modes in EK Cru are the second-order quadrupole mixed mode and the third order dipole pressure mode. A multivariate regression shows a negative correlation of the pulsation amplitude with pulsation frequency, and no statistically significant relationship with the orbital period. In addition, no significant relationship is observed between the pulsation frequency and the orbital period, with the sample showing no significant non-linear coupling between pulsation and orbital parameter in β Cep stars.

Key words. Asteroseismology – Stars: binaries: eclipsing – Stars: oscillations – Stars: massive – Stars: interiors – Stars: rotation

1. Introduction

Massive stars are predominantly found in multiple systems (Sana et al. 2012, 2014; Kobulnicky et al. 2014; Offner et al. 2023). Hence, a substantial fraction ($\geq$ 60%) are expected to be in binaries with over 17% reported to be in eclipsing binaries (Chini et al. 2013). Also, a substantial fraction of the massive eclipsing binaries shows component(s) that are pulsating, which allow us to probe the physics of stellar structure and evolution via combined strengths of eclipsing binary modelling and asteroseismology — see review by Southworth & Bowman (2025). These pulsations manifest in the form of pressure modes (p modes), gravity modes (g modes), mixed modes, Rossby modes (r modes; e.g. Papaloizou & Pringle 1978; Gittins & Andersson 2023), strange modes (e.g. Papaloizou et al. 1997; Saio et al. 1998), and overstable convective modes (Lee 2021). One of the subclasses of massive pulsators that shows some of these pulsations is the β Cep stars, which have masses ranging from about 6 to upwards of 30 $M_\odot$ (Burssens et al. 2020; Fritzewski et al. 2025). These pulsators show predominantly low-radial order p and g modes. This makes them excellent for massive star asteroseismology, enabling one to probe the entire star (see Stankov & Handler 2005; Bowman 2020).

Eclipsing binaries are particularly powerful laboratories for testing stellar structure and evolution theory, since the application of Kepler's laws of motion to their combined light curve and radial velocity time series yields model-independent masses and radii (see Southworth 2021). The absolute numbers of massive pulsators reported in binary or multiple eclipsing systems are significantly smaller compared to their low-mass counterparts (Kirk et al. 2016; IJspeert et al. 2021; Prša et al. 2022). However, since the advent of the Transiting Exoplanet Survey Satellite (TESS) mission (Ricker et al. 2015), there has been a concerted effort to increase the sample size of massive pulsators

⋆ Corresponding author

in eclipsing binaries and conduct ensemble asteroseismology to improve the physics of stellar structure and evolution models. This major barrier of small sample size thus far has hampered the general and ensemble asteroseismic understanding of massive stars. Although not completely solved, the TESS mission has provided the largest to-date catalogue of such stars: 78 β Cep pulsators in eclipsing binaries, among which are 59 new discoveries (e.g. Eze & Handler 2024a,b). These eclipsing binaries containing a β Cep star span different morphological classifications ranging from possible contact to detached binaries, making visualisation of the effect of binary dynamics on pulsation properties in different scenarios. These can also be used to test different scenarios of binary evolution (e.g. pre- and post-interaction).

To date, effectively all asteroseismic analyses of β Cep stars have assumed single-star evolution theory when interpreting the observed pulsation frequencies (e.g. Aerts et al. 2003; Handler et al. 2004; Burssens et al. 2023; Vanlaer et al. 2025). Beyond studies of individual β Cep stars, Fritzewski et al. (2025) conducted ensemble asteroseismic forward modelling of 119 β Cep stars using a combination of *TESS* and *Gaia* light curve data, but the sample only contained three previously known eclipsing binaries. Considering the possible effect of binary dynamics (e.g. orbital angular momentum transport and/or mass transfer) on the pulsational properties of stars, it is not yet clear whether the findings ofFritzewski et al. (2025) properly account for the pulsational properties of β Cep pulsators in eclipsing binaries. Examples of such effects of binarity on the pulsations of β Cep stars include pulsation amplitude dilution of β Cep components in eclipsing binaries (Handler et al. 2005), and tidal suppression of pulsations in close binary systems, such as in the case of δ Sct stars in eclipsing binaries Liakos & Niarchos (2017). However, preliminary results do not show pulsation-orbital periods relation(s) in β Cep stars in eclipsing binaries (Eze et al. 2025) contrary to what is obtainable in δ Sct stars. Moreover, some β Cep stars in close binaries have pulsations that are significantly affected by the equilibrium tide because of a close companion (e.g. Southworth et al. 2020, 2021). All of these studies indicate the need to conduct a detailed ensemble analysis of β Cep stars in eclipsing binaries to decipher the pulsational characteristics of this class of stars in binaries.

In this work, we aim to identify the pulsation modes, where tenable, and investigate the ensemble pulsational characteristics of the sample of β Cep pulsators in eclipsing binaries observed by *TESS* from Eze & Handler (2024b). In Section 2, we describe the sample, its observational properties, and selection criteria. We describe the methods used for pulsation frequency extraction in Section 3. In Section 4, we describe the statistical characterisation of the sample. We describe mode identification procedures in Section 5, discuss tidal synchronisation of the systems in Section 6, discuss the regression analysis of the pulsation and orbital parameters in Section 7, perform asteroseismic modelling of selected cases in Section 8 and conclude in Section 9.

2. Sample Description and Observation

The data sources for this analysis are the catalogue of β Cep stars in eclipsing binaries published by Eze & Handler (2024a) and the 2-min SPOC light curves from the TESS mission (Ricker et al. 2015). In the catalogue, there are 78 reported β Cep pulsators in eclipsing binaries. To obtain a more homogeneous sample and to avoid outliers from unduly driving the results, three systems in the catalogue with no clear orbital period or targets with extremely high pulsation amplitude or extremely long orbital period were removed. Ten other reported β Cep candidates in the catalogue were also excluded in this analysis because their nature could not be explicitly confirmed in the current data. This results in a sample of 65 confirmed β Cep pulsators in eclipsing binaries analysed in this work. The available atmospheric solutions and the absolute parameters of the systems used in this work were obtained predominantly from Eze et al (*A&A* submitted) and with a few obtained from the literature (e.g. Çakırlı et al. 2025).

The 2-min TESS SPOC light curves used for the analysis were extracted from the MAST portal, normalised, and cleaned of systematic and instrumental noise using python scripts. Each sector was independently median-normalised prior to merging. No additional polynomial or spline detrending step was applied, since the subsequent pulsation analysis focused on the range of frequencies $3 - 14\,\mathrm{d}^{-1}$, characteristic of β Cep pulsations and far above the low frequency regime, where residual instrumental or sector-stitching trends are expected to dominate. Only frequencies within the stated range were used for mode-identification or rotational-splitting analysis. In addition, non-finite data points and points that are clearly outliers or noisy are also removed from the light curves prior to prewhitening. In systems where 2-min light curves are unavailable (8 targets), the TESS QLP data (Huang et al. 2020a,b) of the targets are used instead.

3. Pulsation Frequency extraction

Independent pulsations were extracted from the cleaned light curves using star_shadow (IJspeert et al. 2024) and Period04 (Lenz & Breger 2005). Although star_shadow and Period04 are independent pulsation analysis codes, sufficient to provide reliable results, we used them complementarily for validation purposes. For systems in dense fields, with neighbouring stars of comparable magnitudes, where blending is suspected, the accepted prewhitened frequencies from star_shadow were checked with TESS-localise (Higgins & Bell 2022), which localises the likely origin of the pulsation(s), before their acceptance as independent pulsations from the targets. Possible combination frequencies were also removed. Finally, significant β Cep pulsation frequencies that are common to both Star_Shadow and Period04 analyses were accepted as independent pulsations in this work.

Star_shadow in its default configuration considers a frequency significant if the Bayesian Information Criterion (BIC) decreases by 2 (IJspeert et al. 2024; Fritzewski et al. 2025). Although it is capable of analysing blended peaks (IJspeert et al. 2024), it could add noise peaks or many harmonics to the model, resulting in over-extraction of frequencies. For systems in eclipsing binaries, for which Star_shadow is specifically built, this is a benefit as it helps to build more accurately the binary harmonic model and solve the binary orbital dynamics. Although this has the advantage of building binary eclipse models more precisely, it may introduce spurious pulsation frequencies. To reduce this effect, we extracted significant β Cep frequencies using BIC=10 in line with Fritzewski et al. (2025), such that Star_shadow considers a frequency significant only when the BIC decreases by at least 10. This reduces the number of prewhitened frequencies significantly without leaving out significant high amplitude pulsations. Frequencies are adjudged significant in line with Van Beeck et al. (2021). See IJspeert et al. (2024) and Fritzewski et al. (2025) for details of analysis with Star_Shadow. For our analysis with Star_Shadow, the orbital periods reported in Eze & Handler (2024a) were used for the analysis to build the harmonic models, which are subsequently subtracted from the light curves to obtain independent pulsations. The orbital periods of

CD-51 9984 and HD 157400 were taken from Eze et al (submitted).

The pulsation frequencies were also independently prewhitened with Period04, after removing the effect of binarity in the light curves. To this end, a two-fold strategy was adopted. For binaries with orbital periods below 10 d, a 100-frequency multiharmonic fit based on the orbital frequency was computed first, and all signals with an amplitude exceeding a signal-to-noise ratio (S/N) of 3.5 were kept. This heuristic fit was subtracted from the data and the residuals were searched for statistically significant pulsation frequencies, according to the criterion of Baran & Koen (2021). For systems with orbital periods in excess of 10 d, the eclipses were simply removed from the data and only the out-of-eclipse light curves searched for pulsations adopting the same detection criterion.

The search for β Cep frequencies in this analysis was restricted to $3 \leq f \leq 14$ d^{-1} to avoid possible contamination by SPBs and δ Sct pulsations, thereby ensuring that the subsequent analysis was based primarily on β Cep pulsation modes. The list of the accepted significant independent β Cep pulsations used for the subsequent analysis is shown in Appendix A.1.

4. Statistical Characterisation

We examine the statistical distributions of the observed pulsation frequencies and amplitudes across the ensemble. Figure 1 shows histograms of the pulsation frequencies (left panel) and amplitudes (right panel) over-plotted with their Kernel density estimation. Kernel density estimation is a non-parametric method of estimating the probability density function of a random variable (Rosenblatt 1956; Parzen 1962; heng Xie & Wu 2014) and helps to visualise the range and distributions of a random variable. It traces a continuous curve that does not depend on the chosen number of bins like a histogram. As evident in the distribution plots, both the pulsation frequencies and the pulsation amplitudes show unimodal distributions. These suggest that the frequencies and amplitudes are each consistent with being drawn from a single underlying population. Since the amplitude spans multiple orders of magnitude, we used $\log_{10}$ scale for the analysis to reduce dispersion. Both distributions are positively skewed with that of the frequency being more pronounced.

The pulsation frequencies occur mainly in the range of $0.477 - 1.13$ d^{-1} in $\log_{10}$ scale, corresponding to a period range of $3 - 13.51$ d. This is in line with the literature for known apparent single β Cep stars (e.g. Shi et al. 2024). The pulsation frequencies show a modal peak at $\log f \approx 0.749$ ($f \approx 5.53$ d^{-1}) with a median pulsation frequency, $f \approx 6.21$ d^{-1}, resulting in a median pulsation period of $P_{\rm puls} = 1/f \approx 0.16$ d. This is in fairly good agreement with Stankov & Handler (2005) and Pigulski & Pojmański (2009), who studied ensembles of apparently single β Cep stars and found unimodal distributions of the pulsation period with a median pulsation period of approximately 0.17 d. However, while they found a symmetric unimodal distribution around the median, the distribution reported in this work for the pulsation frequency appears to be asymmetric around the median and positively skewed (in both log and nominal scales), thus favouring the observation of lower frequencies compared to higher ones. Radiative damping or geometric cancellation effects at higher frequencies (e.g. Dziembowski 1977; Belkacem et al. 2012) could possibly explain this skewed distribution of pulsations. The departure from normality implies that although pulsations could be approximated (especially the amplitude) to normal distributions, they do not strictly follow normal distributions. The amplitudes, on the other hand, have a median value of approximately 0.76 mmag, respectively, consistent with the prevalence of low amplitude pulsations in β Cep stars.

5. Mode Identification

The pulsation modes of the eclipsing binary systems were identified through the search for rotational multiplets in TESS light-curve data. For β Cep non-radial pulsation modes, the observed frequency of a mode with quantum numbers (n, ℓ, m) is defined, following the perturbative treatment of rotational effects as described by Ledoux (1951) and extended to second order by Dziembowski & Goode (1992), as:

$$f_{n\ell m} = f_{n\ell,0} + m\,(1 - C_{n\ell})\,\Omega + \Omega^2 \left(D_{n\ell} + m^2 E_{n\ell}\right) , \tag{1}$$

where $f_{n\ell m}$ is the observed oscillation frequency of a mode with radial order n, spherical degree ℓ, and azimuthal order m, and $f_{n\ell,0}$ is the corresponding eigenfrequency of the non-rotating star. The quantity Ω denotes the stellar angular rotation rate, the coefficient $C_{n\ell}$ is the Ledoux constant, and the terms $D_{n\ell}$ and $E_{n\ell}$ represent second-order corrections due to centrifugal distortion and higher-order Coriolis effects, respectively. The first-order term $m(1 - C_{n\ell})\Omega$ arises from the Coriolis force and leads to symmetric frequency splitting in a non-magnetic star. The second-order contribution, proportional to Ω^2, includes both a spherically symmetric component $D_{n\ell}$ and an asymmetric component $m^2 E_{n\ell}$, which account for centrifugal distortion and higher-order rotational effects. These second-order terms become significant for moderate to fast rotators and lead to departures from equally spaced multiplets, resulting in asymmetric mode splitting (e.g. Ballot et al. 2010; Bugnet et al. 2021; Guo et al. 2024). For non-magnetic slow and rigidly rotating stars, Eqn. (1) reduces to the first-order perturbative regime, defined as:

$$f_{n\ell m} = f_{n\ell,0} + m \cdot \Omega \cdot (1 - C_{n\ell}) , \tag{2}$$

such that the symmetric frequency spacing between modes of the same n and ℓ, but different m, becomes approximately:

$$\Delta f \approx m \cdot \Omega \cdot (1 - C_{n\ell}) . \tag{3}$$

We plotted schematic Fourier spectra of the extracted pulsation frequencies, in which each detected frequency is represented by a vertical line whose height is proportional to its measured amplitude, and first visually examined the spectra for possible rotational splitting. We further performed a semi-automated pair-wise separation computation and a triplet search to identify the rotational split modes. For a multiplet f_{ijk}, where f_i is the frequency of the retrograde component, f_j the frequency of the zonal mode and f_k the frequency of the prograde component, an asymmetry, $A_s = f_i + f_k - 2f_j$ is estimated. The normalised asymmetry parameter is defined as

$$A_{\rm norm} = \frac{(f_j - f_i) - (f_k - f_j)}{(f_j - f_i) + (f_k - f_j)} \tag{4}$$

which was estimated in accordance with Guo et al. (2024). A multiplet is flagged if the mean spacing is less than unity, which is consistent with the observed splitting of β Cep stars in the literature, and the asymmetry parameter $A \leq 0.1$ d^{-1} such that the normalised asymmetry ≤ 0.05. Table A.1 shows the modes identified in our systems via rotational splitting, and Fig. 2 shows an

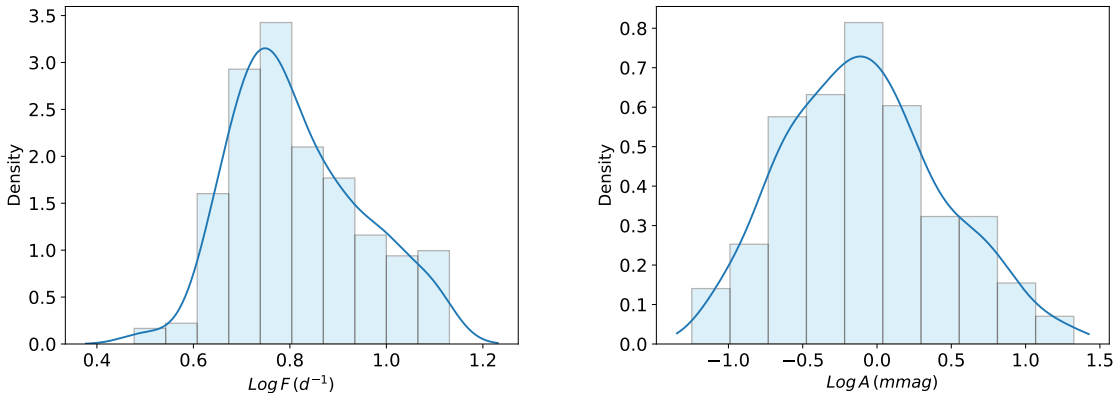

Fig. 1: Distributions of pulsation frequency (left panel) and pulsation amplitude (right panel) in log10 scale.

example of rotational multiplets for one system. There are also systems that show blended modes, which is a situation where two or more observed pulsation frequencies are so close or overlap, often caused by rotation or low frequency resolution of the data making it difficult to resolve individual components (see e.g. Handler 2008; Mirouh 2022) . For such systems, we report modes of higher degree ℓ, or modes of least asymmetry if they are of the same degree. The vertical line Fourier plots for rotational multiplets are shown in Figure A.1 in the Appendix. The asymmetries are also shown in Appendix Table A.1.

Rotational splitting has previously been identified in β Cep stars (e.g. Aerts et al. 2003; Handler et al. 2004; Briquet et al. 2007), which allowed direct mode identification without requiring multicolour photometric data. The splitting also allows direct determination of the interior rotation of stellar systems. Here, splittings are reported in 14 systems with some showing possible mode blends. This blending effect caused by rotation, where, for example, the retrograde component ($-m$) of a quadrupole mode $\ell = 2$ is too close to be resolved from the prograde component ($+m$) of a set of dipole modes ($\ell = 1$), which could be coincidental or points to a possible geometric frequency shifting (e.g. Soufi et al. 1998; Daszyńska-Daszkiewicz et al. 2002).

The rotational frequencies are estimated from the multiplets using Eqn. (2). To do that, we estimate the total spacing of a triplet or quintuplet, Δf_t and divide it by $2m(1 - C_{n\ell})$. Using the information available from a pre-computed grid of massive stars by Vanrespaille et al (A&A submitted), the term $1 - C_{n\ell}$ approximates to 1 for β Cep low-radial order p modes. As a result, we assumed $C_{n\ell} = 0$ for the calculation of our rotational frequency. However, since $C_{n\ell} = 0$ does not always hold, especially for g and mixed modes, the rotation frequency obtained under such an assumption that involves mixed modes is likely underestimated. Where more than one triplet is observed, we computed the rotational frequency for each triplet and if consistent with a solid rotation, the mean rotational frequency is reported for the system. Otherwise, differential rotation is reported. The estimated rotational frequencies are shown in Table A.1. The second-order effect cancels out for frequency differences of modes with $-m$ and $+m$, where m is the same integer.

There are symmetric and asymmetric mode splittings (Handler et al. 2004). The systems within the adopted asymmetric tolerance level are treated as symmetric splitting. Systems that have asymmetric tolerance beyond the adopted threshold but show clear signatures of splitting are treated as asymmetric. Asymmetric rotationally split mode multiplets have recently been discussed in detail in Guo et al. (2024). All the multiplets reported here as shown in Table A.1 are treated as symmetric splitting. The dipole modes ($\ell = 1$) dominate the identified pulsation modes in the sample. Moreover, the majority of the dominant pulsations in most systems are also identified as dipole modes. However, unidentified peaks exist in the sample, and their number is significantly higher than that of identified ones. In addition, we do not rule out the possibility that some identified triplets are incomplete multiplets of a higher degree ℓ. Due to the limited number of identified modes in some of the systems, additional mode identification techniques, such as ground-based multicolour photometry or spectral line profile variability (e.g. see Aerts et al. 1994; Bowman et al. 2022), may be required to conduct robustly identify mode geometries and perform asteroseismic modelling of such targets.

Table A.1 and Fig. A.1 contain four targets that have two dipole ($l = 1$) rotationally split multiplets identified, but the size of their splittings is different (see Figure A.1). There are several possibilities to understand this. For TIC 437617380 (HD 112485) the two spacings are some 20% different and the two modes are very different in frequency, hence they likely sample different parts of the stellar interior. Therefore, TIC 437617380 could be rotating differentially. As it is the higher frequency mode that is more likely to be a pure p mode shows smaller splitting, an alternative explanation in terms of mixed modes is rather unlikely. TIC 355656323 has splittings with an almost similar structure as TIC 437617380 except that the core and the envelope rotate much slower than those of TIC 437617380. In TIC 379012185 (EK Cru), the two splittings are different by about a factor of two and the multiplet centroid frequencies are similar, suggesting that if both modes were $l = 1$ they would sample similar interior regions of the star and have a similar amount of mode mixing. A steep interior rotation gradient explaining the factor of 2 difference also appears implausible. An alternative explanation is that possibly the triplet with the larger spacing is part of an $l = 2$ quintuplet where only the $m \in \{-2, 0, 2\}$ components are observed. This alternative explanation is also supported by the comparison of the asteroseismic model frequencies with the observed ones, which is discussed in Section 8 and shown in Fig. 5, where a model frequency of the $\ell = 2$ mode coincides with the centroid frequency of the multiplet with the larger spacing. The third case with two apparent dipole multiplets split by rotation is TIC 458599043. However, here the two multiplets with similar centroid frequencies have splittings different by about a factor

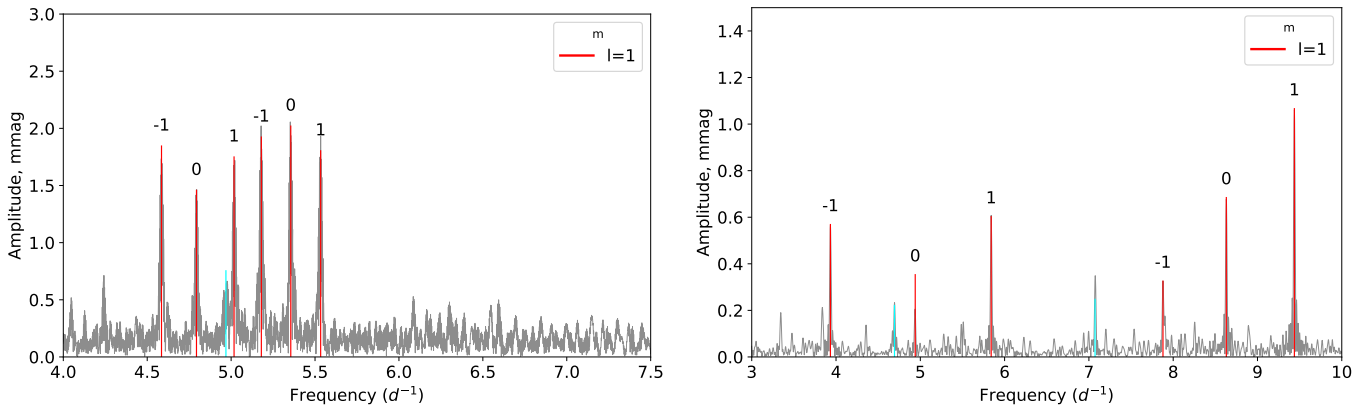

Fig. 2: Example plots showing the rotational multiplets in TIC355656323 (left panel) and TIC437617380 (right panel). The schematic spectra are over-plotted the continuous Fourier spectra.

of 8. For all the arguments mentioned above, we suspect that at least one of these splittings is just a chance agreement.

In addition, while the zonal mode in TIC 458263480 appears to be clear, it is not certain which frequencies correspond to its non-zonal components. Although the higher amplitude frequencies to the left of its selected $m = \pm 1$ components in Fig. A.1 are cut off by our tolerance threshold on asymmetry, they also form a plausible triplet with the identified zonal mode with a rotational frequency comparable to that inferred from the selected multiplet.

6. Rotational synchronisation

We further investigated the synchronicity or otherwise of the rotation of the stars by comparing their rotation periods inferred from their rotational multiplets with their orbital periods. This provides a direct test of the extent to which tidal torques have modified the stellar rotation and allows us to assess whether each system is close to synchronisation. Tidal interactions, in close binary systems, are expected to drive the stellar spin toward synchronisation with the orbital motion and toward circularisation of the orbit (Zahn 1977; Hut 1981). Although both depend on stellar structure, mass ratio, orbital separation, and evolutionary state (e.g. Britavskiy et al. 2024; Sun et al. 2026), they do not always have the same timescales .

Here, we report the synchronicity or otherwise of the systems with identified multiplets. TIC 134522577 and TIC 379012185 show sub-synchronous rotation, while the rotations of TIC 458599043, TIC 355656323 and TIC 269228628 are fairly synchronised with the orbital motion. TIC 28957011. on the other hand, shows a 2:1 spin-orbit resonance (e.g. Schmid et al. 2015) and is likely evolving towards a state of tidal equilibrium. A 2:1 spin-orbit resonance is the situation in which the star rotates twice in one orbital cycle. The rest of the systems show super-synchronous rotation, implying that tidal forces are yet insufficient to synchronise their rotations (see discussion by Southworth & Bowman 2025). Figure 3 shows the plot of the rotational period versus the orbital periods.

Our results do not follow strictly the trends for synchronisation reported in Lennon et al. (2024) in which systems with orbital periods less than 3 d are expected to be synchronised but those with orbital periods more than 10 d are expected to be asynchronous. While synchronisation may be more prevalent among close binary systems with short orbital periods indicating the effects of tidal interaction in synchronisation, systems with orbital period greater than 10 d, TIC 458599043 for example, may also show synchronous rotation. This corroborates the findings that while tidal torque may play a significant role in synchronisation, intrinsic formation processes, efficiency of the angular momentum transport and evolutionary state of the star also contributes to whether a system achieves synchronisation or not (e.g. Levato 1976; Tassoul 1987; Putkuri et al. 2018, 2026).

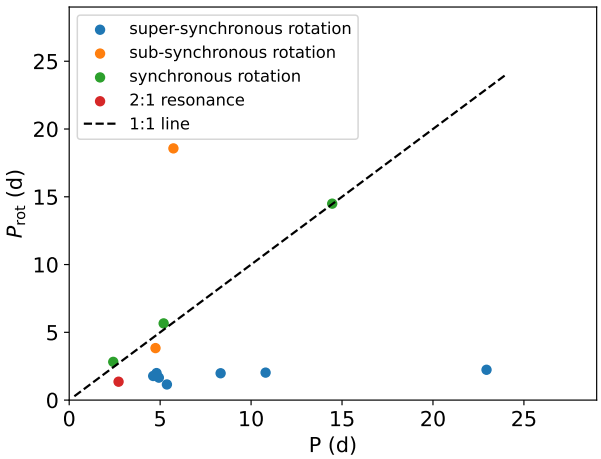

Fig. 3: Plot of rotation period versus orbital period for systems with detected multiplets except TIC 450918869. TIC 450918869 was excluded from the plot owing to its ambiguous rotation profile.

7. Multivariate Regression Analysis

Stellar pulsation amplitudes have been found to be significantly modulated by tidal distortions in binary systems, especially for tidally trapped or triaxial pulsators (Handler et al. 2020; Fuller et al. 2020, 2025). Incidences of tidally excited modes and tidal frequency shifts have also been reported (Fuller & Lai 2011; Bowman et al. 2019; Preece et al. 2019; Guo 2021; Fuller et al. 2025) coupling oscillations and tidal interactions. These modulations and tidally excited oscillations are usually externally induced by centrifugal distortion or corriolis forces. See the review by Southworth & Bowman (2025) for a detailed discussion.

In apparently non-tidally trapped pulsators, several relations have also been reported for certain specific classes of pulsators. Pulsation- and orbital period relationships have been statistically found for δ Sct stars (Soydugan et al. 2006; Kahraman Aliçavuş et al. 2017; Liakos & Niarchos 2017; Liakos 2025), where longer orbital periods are found to correlate with higher pulsation periods. In an ensemble study of β Cep stars, Fritzewski et al. (2025) reported no significant correlation between pulsation amplitude and frequency, although the amplitude of the dominant pulsation mode appears to show a trend with frequency. The preliminary findings of Eze et al. (2025) showed possible exponential decay trends of the amplitude of dominant pulsations with the pulsation frequency and the orbital period, although the significance was not determined. In addition, we expect that the orbital period in the ensemble would be correlated with the pulsation frequency similar to what is observed for δ Sct stars (Liakos 2025). However, this behaviour may be different for β Cep stars. Again, the possible relations between these parameters may not be monotonic as captured by the univariate regression procedures as there could be possible non-linear interactions between the pulsation and orbital parameters.

To quantify the relationships between pulsation and binary orbital parameters, we performed Bayesian multivariate regression analyses using the dominant pulsation frequencies, which appear to be the dominant identified mode multiplets by Fritzewski et al. (2025) and also in this work. We model the logarithmic pulsation amplitude as a function of pulsation frequency and orbital period using a restricted second-order multivariate regression of the form

$$\log A_i = \beta_0 + \beta_1 \log f_i + \beta_2 \log P_i + \beta_3 (\log f_i)(\log P_i) + \epsilon_i \,, \quad (5)$$

where A_i and f_i are the pulsation amplitude and frequency, respectively, P_i is the orbital period, β_0 is the intercept, $\beta_1, \ldots, \beta_n$ are the coefficients and ϵ is Gaussian noise. The model includes an interaction term between the pulsation frequency and the orbital period to capture potential coupling between these parameters. Due to the limited sample size, we performed the analysis with a minimal number of predictors shown in Eqn. (5). Because the amplitude distribution is approximately log-normal, we assumed a normal Gaussian distribution with a Gaussian likelihood and a weakly informative prior. If the likelihood is assumed to be $y_i \sim \mathcal{N}(\mu_i, \sigma_i^2)$, where $y_i = \log A_i$, the mean is given by a linear model $\mu_i = X_i\beta$, and the total variance combines intrinsic scatter and observational uncertainty such that $\sigma_i^2 = \sigma_{\rm int}^2 + \sigma_{{\rm obs},i}^2$. We define the likelihood function explicitly as:

$$\mathcal{L}(y \mid \beta, \sigma_{\rm int}, X) = \prod_{i=1}^{N} \frac{1}{\sqrt{2\pi\sigma_i^2}} \exp\left(-\frac{(y_i - X_i\beta)^2}{2\sigma_i^2} \right) , \quad (6)$$

where $\sigma_{\rm int}$ represents all astrophysical variability that could not be accounted for by the predictors included in the model.

Adopting a weakly informative prior on the regression coefficients, $\beta_j \sim \mathcal{N}(0, \tau^2)$, and a log-uniform prior on the intrinsic scatter, $\log \sigma_{\rm int} \sim \mathcal{U}(-10, 1)$, we defined the posterior distribution as

$$p(\beta, \sigma_{\rm int} \mid y, X) \propto \mathcal{L}(y \mid \beta, \sigma_{\rm int}, X)\, p(\beta, \sigma_{\rm int}) \,, \quad (7)$$

where X is the design matrix containing $\log f$, $\log P$, and their interaction term.

Due to the differences in magnitudes of the input parameters, where, for instance, we have high values for frequency and orbital periods but low values for pulsation amplitude, we standardised the input data to ensure quick convergence. The standardisation is such that the data is centred on zero and scaled to unit variance. This improves efficiency, mixing and numerical stability during MCMC run. Posterior sampling was performed using the No-U-Turn Sampler (NUTS) as implemented in PyMC (Abril-Pla et al. 2023). Figure 4 shows the posterior mean 2D response surface map and uncertainty, respectively, and Table 1 shows the resulting statistical solutions with a posterior predictive p-value of ≈ 0.51 for the models (see Gelman et al. 1996).

From Table 1, it can be seen that the posterior means of the regression coefficients associated with pulsation frequency, orbital period, and their interaction are poorly constrained with very large uncertainties and wide HDI (Highest Density Interval). In contrast, the intercept and the intrinsic scatter are well determined, with the latter suggesting that additional physical factors beyond those included in the model contribute to the observed variability in pulsation amplitudes. No significant correlation is observed between the pulsation amplitude or frequency and the orbital period. This is not unexpected since the periodicities of the low-radial order p modes in β Cep stars are not sub(multiples) of the orbital period. Hence, achieving mode-tidal resonances is harder in this class of pulsations than for higher order g modes where the orbital period and mode periodicities are in the same region of timescales, namely, both of order of days (see Aerts & Tkachenko 2024). However, an indirect dependence could arise through binary evolution. Mass transfer may rejuvenate the mass-accreting component in close binary systems, modifying its internal structure and potentially shifting its pulsation frequencies (see Southworth & Bowman 2025). If such effects are relevant in the current sample, one might expect systematically different pulsation properties among systems with shorter orbital periods. The absence of a significant trend in the present sample may also suggest that such evolutionary effects are weak, not present in most systems, or are masked by the diversity of stellar masses, evolutionary states, and binary interaction histories represented in the sample.

Comparing the complete model to the simplified model obtained under similar conditions but without the interaction term ($\beta_3(\log f_i)(\log P_i)$), using the leave-one-out-cross-validation (LOO), the simplified model is preferred and has a well constrained negative amplitude dependence on the pulsation frequency, but not with the orbital period. The statistical evidence that higher-frequency modes exhibit lower amplitudes is consistent with the observed statistical distribution. The findings in the multivariate analysis are further corroborated by the results of the univariate regression analysis shown in Fig. A.2 obtained under similar conditions with pair-wise use of the parameters.

The findings in this paper on the relation between pulsation and orbital period for β Cep stars do not agree with reports in the literature for δ Sct stars (e.g. Soydugan et al. 2006; Kahraman Aliçavuş et al. 2017; Liakos & Niarchos 2017; Liakos 2025) and the modulation of the amplitude by orbital interaction is also not statistically significant within our sample. Although the models in this analysis capture some trends in the data, the increasing uncertainty at long orbital periods and the poor constraints on the parameters in the model with interaction terms highlight the need for larger samples and improved observational constraints. Future work could incorporate additional physical parameters, such as stellar mass, rotation rate, and metallicity, which are still very limited for β Cep stars in eclipsing binaries. Such extensions would enable a more comprehensive understanding of the interplay between pulsation, rotation, and binarity in mas-

Table 1: Posterior summaries of the Bayesian regression parameters, which include the posterior mean, standard deviation, 94% highest-density interval (HDI), and Gelman–Rubin convergence statistic ($\hat{R}$).

	Mean	SD	94% HDI	$\hat{R}$
Model with interaction				
Intercept(β_0)	0.195	0.067	[0.068, 0.323]	1.0
Pulsation frequency coefficient (β_1)	-0.228	0.139	[-0.489, 0.027]	1.0
Orbital-period coefficient (β_2)	-0.139	0.379	[-0.873, 0.553]	1.0
Interaction coefficient (β_3)	0.126	0.396	[-0.590, 0.904]	1.0
Intrinsic scatter (σ_{int})	0.537	0.049	[0.451, 0.631]	1.0
Simplified model				
Intercept(β_0)	0.195	0.067	[0.068, 0.320]	1.0
Pulsation frequency coefficient (β_1)	-0.189	0.066	[-0.314, -0.067]	1.0
Orbital-period coefficient (β_2)	-0.021	0.067	[-0.146, 0.105]	1.0
Intrinsic scatter (σ_{int})	0.533	0.049	[0.445, 0.626]	1.0

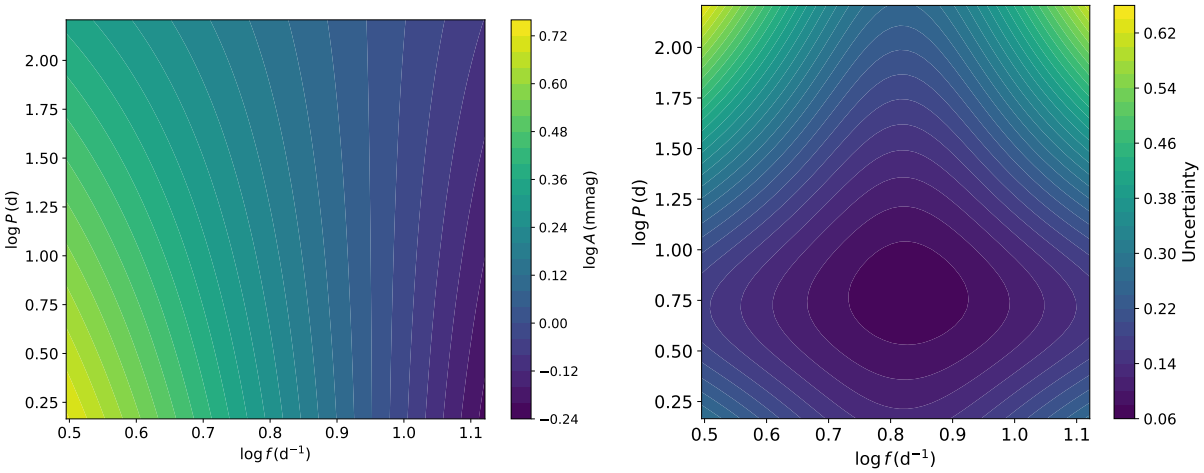

Fig. 4: The left panel shows the relationship among a few pulsation and binary parameters, where P is the orbital period measured in days, f are the pulsation frequencies, and A are the pulsation amplitudes. The model uncertainty is shown in the right panel.

sive stars and would investigate the parameters that contribute to intrinsic variability further.

8. Selected cases of asteroseismic modelling via rotational splitting

We conducted the asteroseismic analysis of two of the candidates (HD 112485 and EK Cru) that show rotational multiplets using Ampharos (Vanrespaille et al. (submitted)) and its accompanying model grid. Ampharos uses MESA (Paxton et al. 2011, 2013, 2015, 2018, 2019; Jermyn et al. 2023) evolutionary and StORM (Vanlaer et al. submitted) pulsation grids of models of varying initial masses, convective boundary mixing with a diffusive exponential prescription, envelope mixing, core hydrogen mass fraction, and rotation to perform the asteroseismic analysis. The grid was computed for a range of $7-29.85\,M_\odot$ for mass, $1-6\,\mathrm{cm^2 s^{-1}}$ for $\log D_{\mathrm{mix}}$, $0.005-0.035$ for f_{ov}, $0.0001-0.701$ for X_c. and $0-0.40$ for $\frac{f_{\mathrm{rot}}}{f_{\mathrm{crit}}}$. While the MESA models are non-rotating, the StORM grid captures the rotation. The latter also captures the distortions to the geometry of the star arising from rotation using the Chandrasekhar-Milne approximation to second order in rotation frequency (Chandrasekhar 1933; Tassoul 1978). Similar to the approach taken by Burssens et al. (2023), Ampharos minimises a χ^2 merit function of a subset of models with a fixed age and rotation frequency that optimally reproduce a favoured zonal mode and the rotational splitting in a star. Its merit function considers the luminosity, effective temperature, identified zonal mode frequencies, and identified rotational splittings. From a weighted average based on the merit function over the subset of models the asteroseismic stellar parameters and interior properties of the stars are derived.

Our selected targets are reported as detached eclipsing binaries of SB1 and SB2, respectively (Çakırlı et al. 2025, Eze et al. (submitted)). Their detached nature allowed us to use the grid of models built for single stars. The selected targets have available stellar parameters and at least two identified modes. Their luminosity and effective temperature used for the analysis were obtained from Eze et al (submitted) and Çakırlı et al. (2025). The identified multiplets in both systems are rotationally split triplets of $\ell = 1$ and 2 modes, leading to the use of a non-radial mode setting in Ampharos. We first searched for the best fit models in the entire β Cep instability strip that reproduce the observed frequency using radial order range of $n_{pg} \in \{-3, -2, ..., +3\}$. In each of the models, a unique n_{pg} that is consistent with the observed zonal modes of the multiplets and the spectroscopic constraints is identified. The identified models are then refitted within a sub-

set of the model grid compatible with the observed spectroscopic parameters.

The uncertainties were estimated from the ensemble of acceptable stellar models obtained during the forward seismic modelling. Models satisfying the adopted spectroscopic constraints were retained and their parameter distributions examined. The likelihood weighting based on χ^2 values obtained from the forward asteroseismic modelling resulted in an effective sample size of approximately one model, producing unrealistically small formal uncertainties. As a result, the final confidence intervals were derived from the unweighted distributions of the accepted models. For each parameter, the lower and upper uncertainties correspond to the 16th and 84th percentiles of the accepted-model ensemble, respectively. Thus, these intervals represent the range of stellar properties consistent with the seismic and spectroscopic constraints within the explored model grid.

The derived asteroseismic parameters of the targets and their uncertainties are shown in Table 2 and the comparison of the observed and seismic model frequencies are shown in Fig. 5. Figure A.3 shows an example plot of the unweighted distributions of mass and radius. As seen in Fig. 5, the observed zonal modes are well reproduced by the models. The two reproduced zonal modes in HD 112485 are the first-order dipole p modes − sensitive to the envelope − and the second-order quadrupole g mode − sensitive to the near-core structure −, respectively, enabling the characterisation of the entire star. Meanwhile, the modes of EK Cru are second-order dipole and quadrupole modes. The derived asteroseismic stellar parameters agree fairly with the observed parameters of the targets (Çakırlı et al. 2025; Nazé et al. 2025), Eze et al (submitted). Nazé et al. (2025) and Eze et al (submitted) obtained a mass of $11.6 \pm 0.6\,M_\odot$ and $11.00 \pm 0.48\,M_\odot$, respectively, for HD 112485, while Çakırlı et al. (2025) obtained a mass of $22.68 \pm 0.04\,M_\odot$ for EK Cru.

We obtain convective core masses of $2.79^{+0.17}_{-0.12}\,M_\odot$ and $8.2^{+0.5}_{-0.6}\,M_\odot$ for HD 112485 and EK Cru, respectively, resulting in core-mass to total mass fractions of 0.264 and 0.373, respectively. These agree with the possible size of the convective core masses for systems of similar masses in the literature (e.g. Tkachenko et al. 2020). The relative mass of the convective core is affected by mass loss, interior mixing, and convective boundary mixing among other processes, and these physical processes increase the relative mass fraction of the core (Maeder 1986; **?**; **?**). Since the core mass is larger for larger stellar mass and/or larger CBM, the higher relative core mass obtained for Ek Cru compared to HD 112485 is expected.

The core hydrogen mass fractions are $0.479^{+0.009}_{-0.010}$ and $0.271^{+0.034}_{-0.037}$, respectively, for HD 112485 and EK Cru, with HD 112485 being less evolved than EK Cru. Although both are of a comparable age, EK Cru has evolved about twice as much compared to HD 112485, which is about half as massive and consistent with the established fact that more massive stars evolve faster. The inferred central hydrogen mass fraction, $X_c = 0.479^{+0.009}_{-0.010}$ reported here for HD 112485 is larger than that reported for any β Cep pulsators subjected to detailed seismic modelling (e.g. Pamyatnykh et al. 2004; Dupret et al. 2004; Briquet et al. 2007; Handler et al. 2009; Aerts et al. 2011; Briquet et al. 2012; Daszyńska-Daszkiewicz et al. 2013; Burssens et al. 2023; Vanlaer et al. 2025), suggesting that the star is the least evolved β Cep stars modelled to date.

The rotation profiles of the models in the grid used by Ampharos are assumed to be uniform (solid-body). So, the rotational frequencies reported for the targets in Table 2 effectively correspond to the best-fitting rotation rates of the models. In systems where differential rotation is suspected, like HD 112485, we optimise the rotation rate from each multiplet individually in Ampharos using the already established best-fit model. By considering the sensitivity region and the difference between the optimised rotation rates, the rotation profile could be adequately described.

Table 2: The derived asteroseismic model parameters of two β Cep stars.

Star	HD 112485	EK Cru
$M\,(M_\odot)$	$10.59^{+0.37}_{-0.23}$	$21.88^{+1.02}_{-0.75}$
$M_{\rm cc}\,(M_\odot)$	$2.794^{+0.168}_{-0.116}$	$8.154^{+0.504}_{-0.603}$
$\frac{M_{\rm cc}}{M}$	$0.264^{+0.009}_{-0.011}$	$0.373^{+0.028}_{-0.029}$
$R\,(R_\odot)$	$5.025^{+0.053}_{-0.039}$	$11.206^{+0.179}_{-0.322}$
X_c	$0.479^{+0.009}_{-0.010}$	$0.271^{+0.034}_{-0.037}$
$f_{\rm ov}$	$0.01^{+0.01}_{-0.01}$	$0.03^{+0.02}_{-0.01}$
$f_{\rm rot}(\mathrm{d}^{-1})$	$0.876^{+0.076}_{-0.012}$	$0.175^{+0.002}_{-0.003}$
$\frac{f_{rot}}{f_{crit}}$	$0.349^{+0.005}_{-0.001}$	$0.151^{+0.1}_{-0.1}$
$\log D_{\rm mix}\,(\mathrm{cm^2\,s^{-1}})$	$1.0^{+2.0}_{-2.0}$	$2.35^{+1.00}_{-2.00}$
$\log L\,(L_\odot)$	$3.954^{+0.037}_{-0.028}$	$5.014^{+0.032}_{-0.024}$
$\log T_{\rm eff}\,(\mathrm{K})$	$4.399^{+0.007}_{-0.006}$	$4.489^{+0.009}_{-0.006}$
$\log$ age (yr)	$7.019^{+0.054}_{-0.035}$	$6.819^{+0.030}_{-0.032}$
$\log g$ (dex)	$4.060^{+0.005}_{-0.004}$	$3.677^{+0.023}_{-0.009}$

The rotational sensitivity kernel (Aerts et al. 2010) is defined as:

$$K_{n\ell}(r) = \frac{\rho(r)\,r^2\left[\xi_r^2(r) + \ell(\ell+1)\,\xi_h^2(r) - 2\,\xi_r(r)\,\xi_h(r) - \xi_h^2(r)\right]}{\int_0^R \rho(r)\,r^2\left[\xi_r^2(r) + \ell(\ell+1)\,\xi_h^2(r)\right]\,\mathrm{d}r} \tag{8}$$

where r denotes the radial coordinate, R the stellar radius, and $\rho(r)$ the density profile. The quantities $\xi_r(r)$ and $\xi_h(r)$ are the radial and horizontal components of the displacement eigenfunction, respectively. The indices ℓ, m and n correspond to the spherical degree, azimuthal order, and radial overtone of the modes, respectively. StORM is used to compute the radial and horizontal displacements.

The higher frequency p mode multiplet in HD 112485 with the zonal mode frequency $f = 8.6304\ \mathrm{d}^{-1}$ gives an envelope rotational frequency of $0.6909^{+0.0010}_{-0.0009}\ \mathrm{d}^{-1}$, while the rotation rate of the lower frequency multiplet, which is more sensitive to the near-core region, could not be well constrained independently. However, the discrepancy between the envelope-sensitive rotational frequency and the inferred solid body rotation suggests that the near-core-sensitive multiplet may be probing a faster-rotating interior, with a faster rotation frequency $> 0.69098\ \mathrm{d}^{-1}$ and possibly indicating differential rotation. The inferred envelope rotation from the forward asteroseismic model for HD 112485 is in agreement with surface rotation derived from spectroscopy (see, Eze et al, submitted).

The sensitivity kernels are shown in Fig. 6 for HD 112485 (left panel) and EK Cru (middle and right panels). The zonal

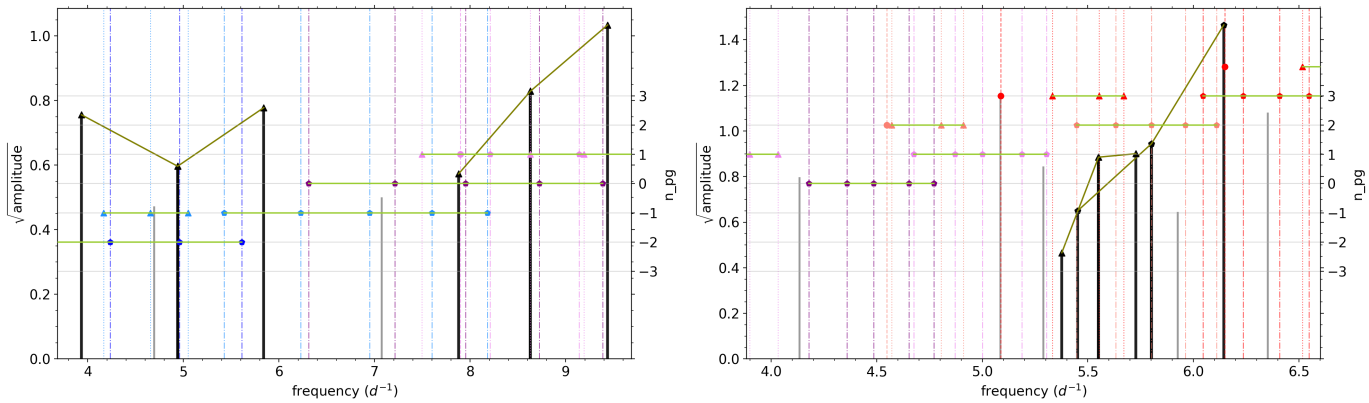

Fig. 5: Comparison of observed and best-fit model pulsation frequencies of HD 112485 (left panel) and EK Cru (right panel). Identified modes are in black and the unidentified modes are in gray. Other coloured lines denote model mode frequencies of different angular degrees. Triangles denote dipole modes, diamonds denote quadrupole modes and circles denote radial modes.

mode frequency of $f = 8.6304$ d^{-1} in HD 112485 is sensitive to a broad part in the envelope of the star, which is characteristic of p modes. In EK Cru, the frequency of the zonal mode, $f = 5.8017$ d^{-1}, is sensitive to both the near-core region and the envelope, characteristic of a mixed mode. It is a low-radial order mixed mode with a substantial g-mode character and appreciable sensitivity to the outer envelope, and thus samples both the core and the envelope, while $f = 5.5505$ d^{-1} samples only the envelope. However, both the core and the envelope have similar rotational frequencies, and are compatible with a quasi-rigid rotation of the primaries of the systems.

9. Conclusions

We conducted an ensemble pulsation study of a sample of 65 β Cep pulsators in eclipsing binaries, as well as in-depth asteroseismic analysis of two selected cases in the sample. We determined the distribution of the pulsational properties, identified the pulsational mode characteristics, inferred the statistical relations between the pulsation and binary parameters, and derived the asteroseismic parameters of HD 112485 and EK Cru.

The distributions of the pulsation frequencies and amplitudes are unimodal and positively skewed. The identified modes are predominantly dipole modes, with some systems showing synchronous, 2:1 resonance, sub-synchronous, and super-synchronous rotation rates. Some systems are also observed to show differential rotation, but the majority of the systems with identified multiplets show quasi-rigid rotation. The pulsation amplitude of the systems in the sample appears to have an anti-correlation with the pulsation frequency but shows no significant correlation with the orbital period. The frequency also shows no significant relation to the orbital period in the current sample. The interior properties of two β Cep stars were asteroseismically derived, yielding convective core masses of 2.714 $M_\odot$ for the 10.59 $M_\odot$ star HD 112485 and 8.154 $M_\odot$ for the 21.88 $M_\odot$ star EK Cru. The evolutionary states, interior mixing, and rotation profiles are also reported.

Acknowledgements. This work was supported by the Polish National Science Foundation (NCN) under grant nr. 2021/43/B/ST9/02972 led by GH. CIE thanks the Polish National Agency for Academic Exchange (NAWA) for funding, through the Bekker NAWA grant number BPN/BEK/2024/1/00049, the internship where part of this work was conducted. The author also thanks A. Miszuda for helpful comments. DMB gratefully acknowledges UK Research and Innovation (UKRI) in the form of a Frontier Research grant under the UK government's ERC Horizon Europe funding guarantee (SYMPHONY; PI Bowman; grant number: EP/Y031059/1), and a Royal Society University Research Fellowship (PI Bowman; grant number: URF\R1\231631). CA and AK acknowledge financial support from the Flemish Government under the long-term structural Methusalem funding programme by means of the project SOUL: Stellar evolution in full glory, grant METH/24/012. MV received funding from the KU Leuven Research Council (doctoral mandate grant DB/24/008). MV and CA acknowledge financial support from the European Research Council (ERC) under the Horizon Europe programme (Synergy Grant agreement N◦101071505: 4D-STAR). While partially funded by the European Union, views and opinions expressed are however those of the authors only and do not necessarily reflect those of the European Union or the European Research Council. Neither the European Union nor the granting authority can be held responsible for them. AT acknowledges support from the BELgian federal Science Policy Office (BELSPO) through PRODEX grant PLATO (ZKE8588), and from the Research Foundastion – Flanders (FWO) (grant agreement G0ABL24N).This paper used the TESS data obtained from the Mikulski Archive for Space Telescopes (MAST) at the Space Telescope Science Institute. Support to MAST for these data is provided by the NASA Office of Space Science via grant NAG5-7584 and by other grants and contracts. Funding for the TESS mission is provided by the NASA Explorer Programme.

References

Abril-Pla, O., Andreani, V., Carroll, C., et al. 2023, PeerJ Computer Science, 9, e1516
Aerts, C., Briquet, M., Degroote, P., Thoul, A., & van Hoolst, T. 2011, A&A, 534, A98
Aerts, C., Christensen-Dalsgaard, J., & Kurtz, D. W. 2010, Asteroseismology (Springer Science+Business Media B.V.)
Aerts, C., Lehmann, H., Briquet, M., et al. 2003, A&A, 399, 639
Aerts, C., Mathias, P., Gillet, D., & Waelkens, C. 1994, A&A, 286, 109
Aerts, C. & Tkachenko, A. 2024, A&A, 692, R1
Ballot, J., Lignières, F., Reese, D. R., & Rieutord, M. 2010, A&A, 518, A30
Baran, A. S. & Koen, C. 2021, Acta Astron., 71, 113
Belkacem, K., Dupret, M. A., Baudin, F., et al. 2012, A&A, 540, L7
Bowman, D. M. 2020, Frontiers in Astronomy and Space Sciences, 7, 70
Bowman, D. M., Johnston, C., Tkachenko, A., et al. 2019, ApJ, 883, L26
Bowman, D. M., Vandenbussche, B., Sana, H., et al. 2022, A&A, 658, A96
Briquet, M., Morel, T., Thoul, A., et al. 2007, MNRAS, 381, 1482
Briquet, M., Neiner, C., Aerts, C., et al. 2012, MNRAS, 427, 483
Britavskiy, N., Renzo, M., Nazé, Y., Rauw, G., & Vynatheya, P. 2024, A&A, 684, A35
Bugnet, L., Prat, V., Mathis, S., et al. 2021, A&A, 650, A53
Burssens, S., Bowman, D. M., Michielsen, M., et al. 2023, Nature Astronomy, 7, 913
Burssens, S., Simón-Díaz, S., Bowman, D. M., et al. 2020, A&A, 639, A81
Çakırlı, Ö., Hoyman, B., Özdarcan, O., & Bilir, S. 2025, MNRAS, 543, 2958
Chandrasekhar, S. 1933, MNRAS, 93, 390
Chini, R., Barr, A., Buda, L. S., et al. 2013, Central European Astrophysical Bulletin, 37, 295
Daszyńska-Daszkiewicz, J., Dziembowski, W. A., Pamyatnykh, A. A., & Goupil, M.-J. 2002, A&A, 392, 151

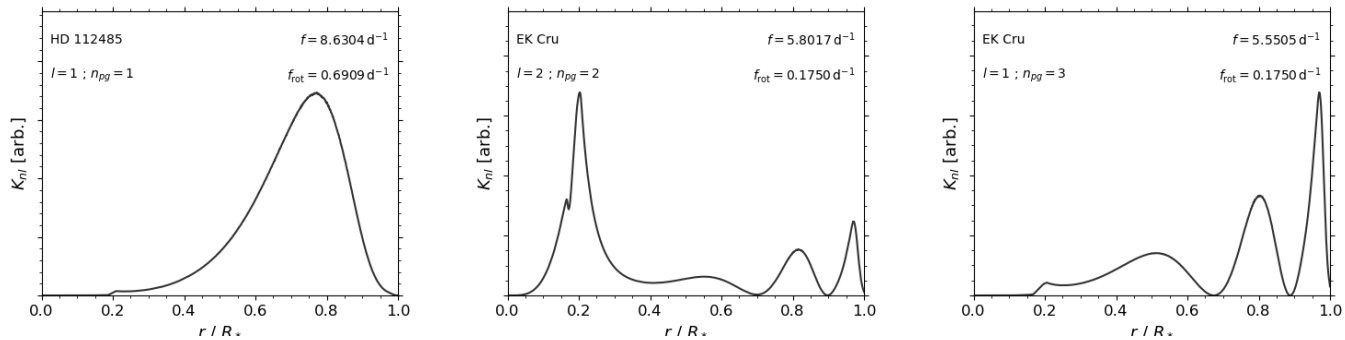

Fig. 6: Plots showing the rotational sensitivity kernel of HD 112485 (left panel) and EK Cru (middle and right panels).

Daszyńska-Daszkiewicz, J., Szewczuk, W., & Walczak, P. 2013, MNRAS, 431, 3396
Dupret, M. A., Thoul, A., Scuflaire, R., et al. 2004, A&A, 415, 251
Dziembowski, W. 1977, Acta Astron., 27, 203
Dziembowski, W. A. & Goode, P. R. 1992, ApJ, 394, 670
Eze, C. I. & Handler, G. 2024a, ApJS, 272, 25
Eze, C. I. & Handler, G. 2024b, Contributions of the Astronomical Observatory Skalnate Pleso, 54, 70
Eze, C. I., Handler, G., Kahraman Aliçavuş, F., Pawar, T., & Miszuda, A. 2025, Contributions of the Astronomical Observatory Skalnate Pleso, 55, 452
Fritzewski, D. J., Vanrespaille, M., Aerts, C., et al. 2025, A&A, 698, A253
Fuller, J., Kurtz, D. W., Handler, G., & Rappaport, S. 2020, MNRAS, 498, 5730
Fuller, J. & Lai, D. 2011, MNRAS, 412, 1331
Fuller, J., Rappaport, S., Jayaraman, R., Kurtz, D., & Handler, G. 2025, ApJ, 979, 80
Gelman, A., Meng, X.-L., & Stern, H. 1996, Statistica sinica, 733
Gittins, F. & Andersson, N. 2023, Monthly Notices of the Royal Astronomical Society, 521, 3043
Guo, Z. 2021, Frontiers in Astronomy and Space Sciences, Volume 8 - 2021
Guo, Z., Bedding, T. R., Pamyatnykh, A. A., et al. 2024, arXiv e-prints, arXiv:2406.15678
Handler, G. 2008, Communications in Asteroseismology, 157, 106
Handler, G., Kurtz, D. W., Rappaport, S. A., et al. 2020, Nature Astronomy, 4, 684
Handler, G., Matthews, J. M., Eaton, J. A., et al. 2009, ApJ, 698, L56
Handler, G., Shobbrook, R. R., Jerzykiewicz, M., et al. 2004, MNRAS, 347, 454
Handler, G., Shobbrook, R. R., & Mokgwetsi, T. 2005, MNRAS, 362, 612
heng Xie, X. & Wu, J. 2014, Applied Mathematics-a Journal of Chinese Universities Series B, 2014, 1684
Higgins, M. E. & Bell, K. J. 2022, arXiv e-prints, arXiv:2204.06020
Huang, C. X., Vanderburg, A., Pál, A., et al. 2020a, Research Notes of the American Astronomical Society, 4, 204
Huang, C. X., Vanderburg, A., Pál, A., et al. 2020b, Research Notes of the American Astronomical Society, 4, 206
Hut, P. 1981, A&A, 99, 126
IJspeert, L. W., Tkachenko, A., Johnston, C., et al. 2021, A&A, 652, A120
IJspeert, L. W., Tkachenko, A., Johnston, C., et al. 2024, A&A, 685, A62
Jermyn, A. S., Bauer, E. B., Schwab, J., et al. 2023, ApJS, 265, 15
Kahraman Aliçavuş, F., Soydugan, E., Smalley, B., & Kubát, J. 2017, Monthly Notices of the Royal Astronomical Society, 470, 915
Kirk, B., Conroy, K., Prša, A., et al. 2016, AJ, 151, 68
Kobulnicky, H. A., Kiminki, D. C., Lundquist, M. J., et al. 2014, ApJS, 213, 34
Ledoux, P. 1951, ApJ, 114, 373
Lee, U. 2021, MNRAS, 505, 1495
Lennon, D. J., Dufton, P. L., Villaseñor, J. I., et al. 2024, A&A, 688, A141
Lenz, P. & Breger, M. 2005, Communications in Asteroseismology, 146, 53
Levato, H. 1976, ApJ, 203, 680
Liakos, A. 2025, Contributions of the Astronomical Observatory Skalnate Pleso, 55, 172
Liakos, A. & Niarchos, P. 2017, MNRAS, 465, 1181
Maeder, A. 1986, in IAU Symposium, Vol. 116, Luminous Stars and Associations in Galaxies, ed. C. W. H. De Loore, A. J. Willis, & P. Laskarides, 287–299
Mirouh, G. M. 2022, Frontiers in Astronomy and Space Sciences, Volume 9 - 2022
Nazé, Y., Rauw, G., Kołaczek-Szymański, P. A., Britavskiy, N., & Labadie-Bartz, J. 2025, A&A, 703, A239
Offner, S. S. R., Moe, M., Kratter, K. M., et al. 2023, in Astronomical Society of the Pacific Conference Series, Vol. 534, Protostars and Planets VII, ed. S. Inutsuka, Y. Aikawa, T. Muto, K. Tomida, & M. Tamura, 275
Pamyatnykh, A. A., Handler, G., & Dziembowski, W. A. 2004, Monthly Notices of the Royal Astronomical Society, 350, 1022
Papaloizou, J. & Pringle, J. E. 1978, MNRAS, 182, 423
Papaloizou, J. C. B., Alberts, F., Pringle, J. E., & Savonije, G. J. 1997, MNRAS, 284, 821
Parzen, E. 1962, The Annals of Mathematical Statistics, 33, 1065
Paxton, B., Bildsten, L., Dotter, A., et al. 2011, ApJS, 192, 3
Paxton, B., Cantiello, M., Arras, P., et al. 2013, ApJS, 208, 4
Paxton, B., Marchant, P., Schwab, J., et al. 2015, ApJS, 220, 15
Paxton, B., Schwab, J., Bauer, E. B., et al. 2018, ApJS, 234, 34
Paxton, B., Smolec, R., Schwab, J., et al. 2019, ApJS, 243, 10
Pigulski, A. & Pojmański, G. 2009, in American Institute of Physics Conference Series, Vol. 1170, Stellar Pulsation: Challenges for Theory and Observation, ed. J. A. Guzik & P. A. Bradley, 351–354
Preece, H. P., Jeffery, C. S., & Tout, C. A. 2019, Monthly Notices of the Royal Astronomical Society, 489, 3066
Prša, A., Kochoska, A., Conroy, K. E., et al. 2022, ApJS, 258, 16
Putkuri, C., Gamen, R., Morrell, N. I., et al. 2026, A&A, 706, A311
Putkuri, C., Gamen, R., Morrell, N. I., et al. 2018, A&A, 618, A174
Ricker, G. R., Winn, J. N., Vanderspek, R., et al. 2015, Journal of Astronomical Telescopes, Instruments, and Systems, 1, 014003
Rosenblatt, M. 1956, The Annals of Mathematical Statistics, 27, 832
Saio, H., Baker, N. H., & Gautschy, A. 1998, Monthly Notices of the Royal Astronomical Society, 294, 622
Sana, H., de Mink, S. E., de Koter, A., et al. 2012, Science, 337, 444
Sana, H., Le Bouquin, J. B., Lacour, S., et al. 2014, ApJS, 215, 15
Schmid, V. S., Tkachenko, A., Aerts, C., et al. 2015, A&A, 584, A35
Shi, X.-d., Qian, S.-b., Zhu, L.-y., et al. 2024, ApJS, 271, 28
Soufi, F., Goupil, M.-J., & Dalsgaard, J. C. 1998, A&A, 334, 911
Southworth, J. 2021, Universe, 7, 369
Southworth, J. & Bowman, D. 2025, arXiv e-prints, arXiv:2509.08426
Southworth, J., Bowman, D. M., & Pavlovski, K. 2021, MNRAS, 501, L65
Southworth, J., Bowman, D. M., Tkachenko, A., & Pavlovski, K. 2020, MNRAS, 497, L19
Soydugan, E., İbanoğlu, C., Soydugan, F., Akan, M. C., & Demircan, O. 2006, Monthly Notices of the Royal Astronomical Society, 366, 1289
Stankov, A. & Handler, G. 2005, ApJS, 158, 193
Sun, M., Xia, H., Gossage, S., et al. 2026, The Astrophysical Journal, 998, 32
Tassoul, J. 1978, Lucy: For rotating protostars, much of the infailing outer envel
Tassoul, J.-L. 1987, ApJ, 322, 856
Tkachenko, A., Pavlovski, K., Johnston, C., et al. 2020, A&A, 637, A60
Van Beeck, J., Bowman, D. M., Pedersen, M. G., et al. 2021, A&A, 655, A59
Vanlaer, V., Bowman, D. M., Burssens, S., et al. 2025, A&A, 701, A5
Zahn, J. P. 1977, A&A, 57, 383

Appendix A: Rotational multiplets of β Cep eclipsing binaries in TESS data

Here, we include additional relevant Tables and Figures.

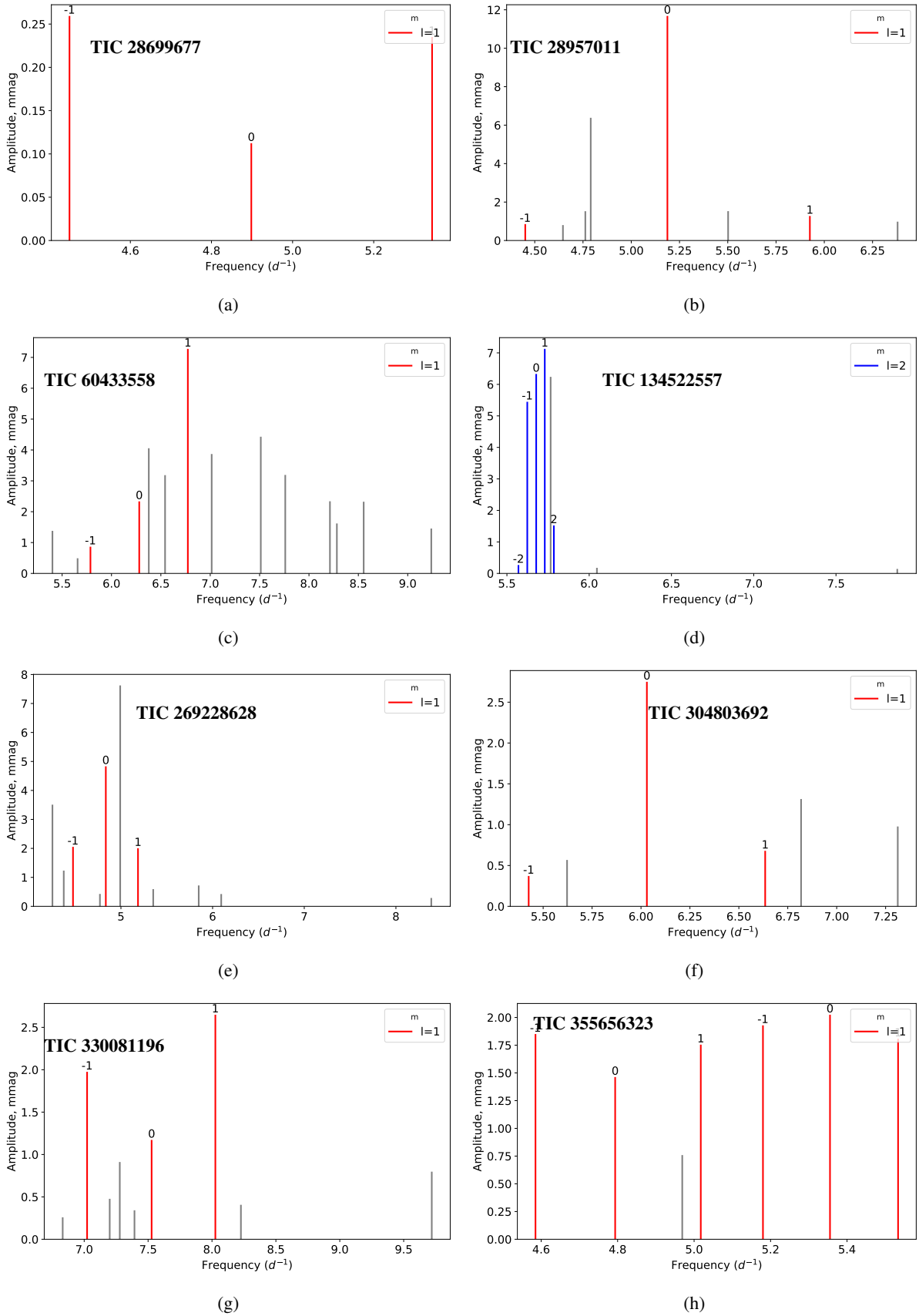

(a) (b) (c) (d) (e) (f) (g) (h)

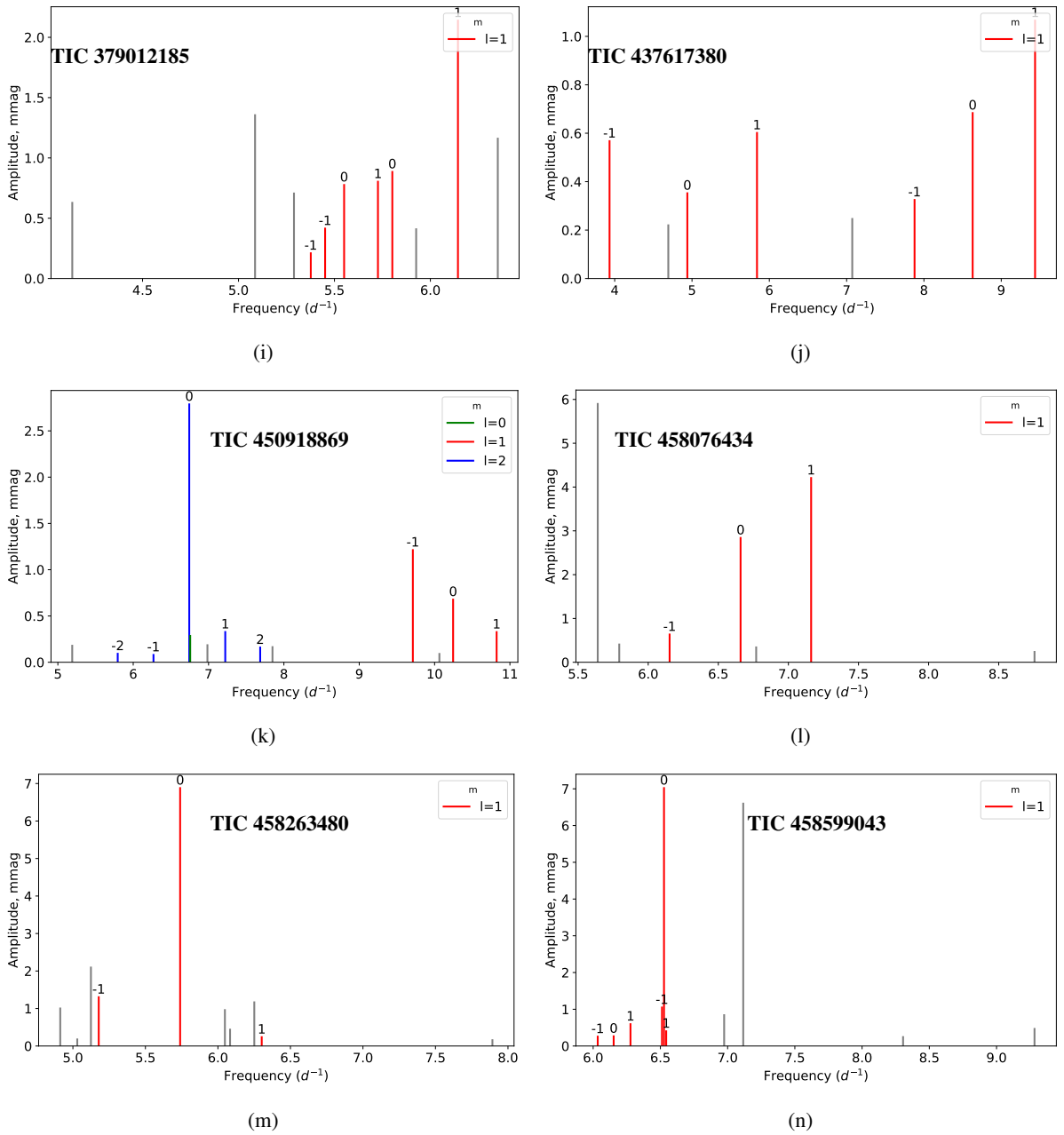

Fig. A.1: Systems with rotational multiplets.

Table A.1: Independent β Cep pulsation frequencies and amplitudes of the systems showing rotational multiplets, where ℓ is the spherical degree and m is the azimuthal order. Spacing is Δf_{ij} and Δf_{jk}. Accepted significant independent β Cep pulsations used for the analysis in this work is shown via the link *list of pulsations*. The first frequency in the online table represents the dominant pulsation in each target

TIC ID	P (d)	f (d^{-1})	A (mmag)	ℓ	m	spacing d^{-1}	$[A_s\, d^{-1}; A_{\rm norm}]$	$f_{\rm rot}$ (d^{-1})
28699677	22.9444(5)							
		4.44995(3)	0.26(1)	1	-1	0.4483		
		4.89821(7)	0.11(1)	1	0		[0.0025; 0.003]	0.44698(5)
		5.34393(3)	0.24(1)	1	1	0.4457		
28957011	2.7139(1)							
		4.451(2)	0.9(1)	1	-1	0.7364		
		5.1873(1)	11.7(1)	1	0		[0.0016; 0.001]	0.737(1)
		5.925(1)	1.3(1)	1	1	0.73799		
		5.5018(9)	1.5(1)					

Continued on next page

TIC ID	P (d)	f (d^{-1})	A (mmag)	ℓ	m	spacing d^{-1}	$[A_s\, d^{-1}; A_{\rm norm}]$	$f_{\rm rot}$ (d^{-1})
		4.7621(9)	1.5(1)					
		6.379(2)	0.9(1)					
		4.646(2)	0.8(1)					
		4.79005(2)	6.4(1)					
60433558	10.798(1)							
		5.786807(6)	0.87(1)	1	-1	0.4941		
		6.280927(2)	2.33(1)	1	0		[0.0018; 0.002]	0.493238(3)
		6.7732821(7)	7.28(1)	1	1	0.4924		
		7.512030(1)	4.43(1)					
		6.377774(1)	4.06(1)					
		7.014646(1)	3.87(1)					
		7.759924(2)	3.19(1)					
		6.542596(2)	3.18(1)					
		8.212493(2)	2.34(1)					
		8.554092(2)	2.32(1)					
		8.282639(3)	1.62(1)					
		9.238721(4)	1.45(1)					
		5.401952(4)	1.38(1)					
		5.65661(1)	0.49(1)					
134522557	5.730(2)							
		5.57001(1)	0.27(2)	2	-2	0.1079		
		5.6237481(7)	5.45(2)	2	-1	0.0542		
		5.6779561(6)	6.33(2)	2	0		[0.0021, 0.0005;	0.053844(3)
		5.7300571(5)	7.13(2)	2	1	0.0521	0.02, 0.002]	
		5.785393(3)	1.52(2)	2	2	0.1074		
		5.7657150(6)	6.24(2)					
		6.04692(2)	0.18(2)					
		7.87248(3)	0.14(2)					
269228628	2.422(1)							
		4.477037(4)	2.05(2)	1	-1	0.3579		
		4.835017(1)	4.83(2)	1	0		[0.0068; 0.009]	0.354582(3)
		5.186201(4)	2.00(2)	1	1	0.3512		
		4.9918992(9)	7.62(2)					
		4.252738(2)	3.51(2)					
		4.376108(6)	1.23(2)					
		5.84860(1)	0.72(2)					
		5.35212(1)	0.59(2)					
		4.77074(2)	0.43(2)					
		6.09405(2)	0.42(2)					
		8.38589(3)	0.29(2)					
304803692	4.92870(2)							
		5.426(2)	0.37(3)	1	-1	0.6039		
		6.0300(2)	2.75(3)	1	0		[0.0006; 0.0005]	0.604(1)
		6.6346(9)	0.68(3)	1	1	0.6046		
		6.8180(6)	1.31(3)					
		7.3121(5)	0.98(3)					
		5.622(1)	0.57(3)					
330081196	4.80323(6)							
		6.83178(5)	0.26(2)	1	-1			
		7.022813(6)	1.98(2)	1	-1	0.5048		
		7.52762(1)	1.17(2)	1	0		[0.006; 0.006]	0.59951(3)
		8.026362(5)	2.65(2)	1	1	0.4987		
		8.22630(3)	0.41(2)	1	1			
		9.71971(2)	0.79(2)					
		7.19968(3)	0.48(2)					
		7.39349(4)	0.34(2)					
		7.27848(1)	0.91(2)					
355656323	5.1929(1)							
		5.18011(1)	1.93(4)	1	-1	0.1753		
		5.35544(1)	2.02(4)	1	0		[0.0027; 0.008]	0.17669(1)
		5.53351(1)	1.81(4)	1	1	0.1781		

Continued on next page

TIC ID	P (d)	f (d^{-1})	A (mmag)	ℓ	m	spacing d^{-1}	$[A_s\, d^{-1}; A_{\rm norm}]$	$f_{\rm rot}$ (d^{-1})
		4.58521(1)	1.85(4)	1	-1	0.3838		
		4.79358(2)	1.46(4)	1	0		[0.0026; 0.0034]	0.38510(1)
		5.01749(1)	1.75(4)	1	1	0.3864		
		4.96904(3)	0.76(4)					
379012185	4.7447(1)							
		5.4513(3)	0.422(7)	1	-1	0.3503		
		5.8017(2)	0.892(7)	1	0		[0.0083; 0.01]	
		6.14371(7)	2.146(7)	1	1	0.342		0.1751(4)
		5.3767(6)	0.217(7)	1	-1	0.1737		
		5.5505(2)	0.783(7)	1	0		[0.0026; 0.007]	
		5.7268(2)	0.810(7)	1	1	0.1763		
		5.0863(1)	1.362(7)					
		6.3514(1)	1.168(7)					
		5.2891(2)	0.713(7)					
		4.1337(2)	0.635(7)					
		5.9259(3)	0.416(7)					
437617380	5.372(1)							
		7.8788(6)	0.33(2)	1	-1	0.7516		
		8.6304(3)	0.69(2)	1	0		[0.0557; 0.04]	
		9.4377(2)	1.07(2)	1	1	0.8073		0.8666(7)
		3.9334(3)	0.57(2)	1	-1	1.0062		
		4.9396(7)	0.36(2)	1	0		[0.1; 0.05]	
		5.8408(3)	0.61(2)	1	1	0.9012		
		7.0730(8)	0.25(2)					
		4.6935(8)	0.22(2)					
450918869	4.222(5)							
		6.75639(2)	0.29(1)	0				
		5.79438(5)	0.10(1)	2	-2	0.9495		
		6.26911(5)	0.09(1)	2	-1	0.4748		
		6.743891(2)	2.79(1)	2	0		[0.003, 0.008;	0.47275(1)
		7.22166(1)	0.34(1)	2	1	0.4778	0.003, 0.004]	
		7.68537(3)	0.17(1)	2	2	0.9415		
		9.711631(4)	1.22(1)	1	-1	0.534		
		10.245958(7)	0.69(1)	1	0		0.044	0.556(2)
		10.82348(1)	0.34(1)	1	1	0.578		
		6.98505(2)	0.19(1)					
		7.84854(3)	0.17(1)					
		10.06382(5)	0.10(1)					
		5.19053(2)	0.19(1)					
458076434	8.3249(8)							
		6.15265(3)	0.65(3)	1	-1	0.5062		
		6.658866(7)	2.86(3)	1	0		[0.003; 0.003]	0.50470(2)
		7.162049(5)	4.23(3)	1	1	0.5032		
		5.640013(3)	5.92(3)					
		5.79341(5)	0.43(3)					
		6.77019(6)	0.36(3)					
		8.75539(8)	0.26(3)					
458263480	4.618(1)							
		5.17808(1)	1.33(2)	1	-1	0.5613		
		5.739375(2)	6.90(2)	1	0		[0.0013; 0.001]	0.56195(3)
		6.30198(6)	0.26(2)	1	1	0.5626		
		5.124229(9)	2.12(2)					
		6.25069(1)	1.19(2)					
		4.91264(2)	1.03(2)					
		6.04805(2)	0.98(2)					
		6.08365(4)	0.46(2)					
		5.03004(8)	0.20(2)					
		7.89274(9)	0.18(2)					
458599043	14.46(2)							
		6.51201(3)	1.07(5)	1	-1	0.0149		
		6.526882(5)	7.04(5)	1	0		[0.0014; 0.04]	

Continued on next page

TIC ID	P (d)	f (d^{-1})	A (mmag)	ℓ	m	spacing d^{-1}	$[A_s\, d^{-1}; A_{\rm norm}]$	$f_{\rm rot}$ (d^{-1})
		6.54317(9)	0.43(5)	1	1	0.0163		0.069(1)
		6.0341(1)	0.28(5)	1	-1	0.1185		
		6.1525(1)	0.29(5)	1	0		[0.0066; 0.03]	
		6.27761(6)	0.62(5)	1	1	0.1251		
		7.116112(6)	6.62(5)					
		6.97419(4)	0.86(5)					
		9.28237(8)	0.49(5)					
		8.3049(1)	0.27(5)					

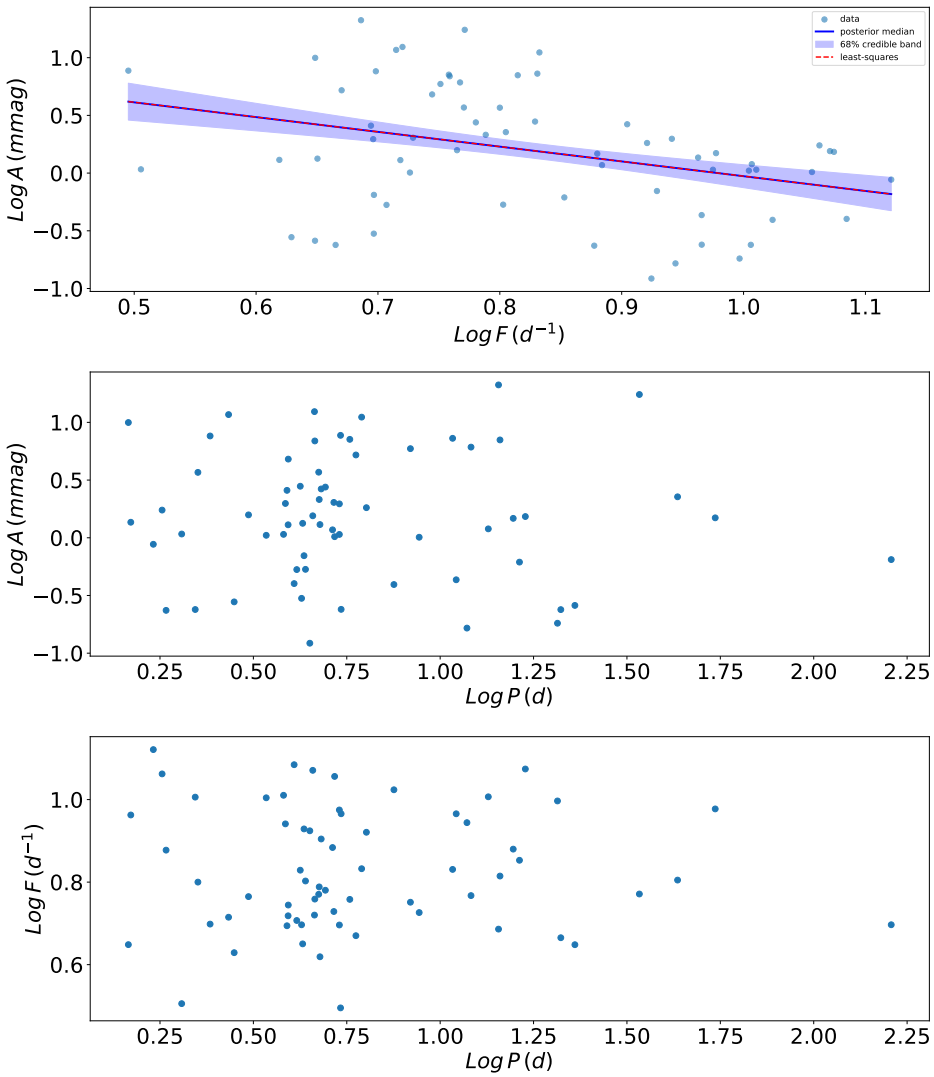

Fig. A.2: Results of the univariate regression analysis between orbital and pulsation parameters. The ordinary least-squares fit in top panel yielded a Pearson correlation coefficient $r = -0.35$ with a frequentist p-value of = 0.005.

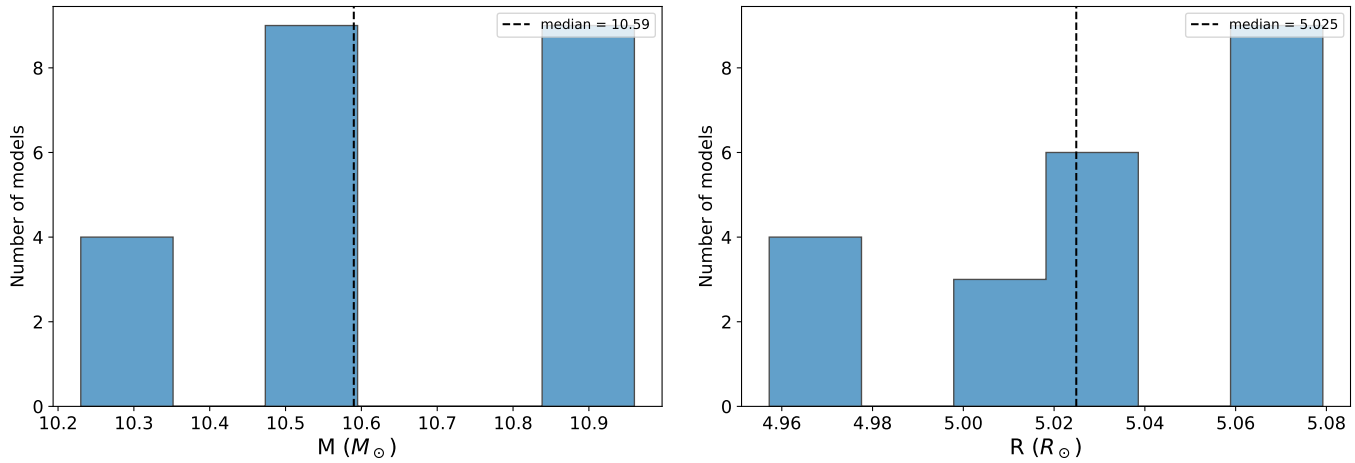

Fig. A.3: Example plots of the unweighted distributions of the derived parameters. The distributions of mass (left panel) and radius (right panel) of HD 112485 are shown for the χ^2 models compatible with the spectroscopic constraints. The gaps in the unweighted distributions reflect the discrete sampling of the stellar-model grid and the subsequent selection of only models satisfying the adopted constraints. They are therefore not interpreted as evidence for physically distinct populations.